THE JOURNAL OF BIOLOGICAL CHEMISTRY
Vol. 276, No. 9, Issue of March 2, pp. 6151–6160, 2001
Printed in U.S.A.
© 2001 by The American Society for Biochemistry and Molecular Biology, Inc.

Location of the Polyamine Binding Site in the Vestibule of the Nicotinic Acetylcholine Receptor Ion Channel*

Received for publication, September 15, 2000, and in revised form, December 1, 2000
Published, JBC Papers in Press, December 4, 2000, DOI 10.1074/jbc.M008467200

M. Gabriele Bixel‡, Christoph Weise‡, Maria L. Bolognesi§, Michela Rosini§, Matthew J. Brierly¶, Ian R. Mellor¶, Peter N. R. Usherwood¶, Carlo Melchiorre§, and Ferdinand Hucho‡‖

From the ‡Institut für Chemie-Biochemie (AG Neurochemie), Fachbereich Biologie, Chemie, Pharmazie, Freie Universität Berlin, 14195 Berlin, Germany, §Dipartimento di Scienze Farmaceutiche, Università di Bologna, 40125 Bologna, Italy, and ¶Division of Molecular Toxicology, School of Biology, University Park, University of Nottingham, Nottingham NG7 2RD, United Kingdom

To map the structure of a ligand-gated ion channel, we used the photolabile polyamine-containing toxin MR44 as photoaffinity label. MR44 binds with high affinity to the nicotinic acetylcholine receptor in its closed channel conformation. The binding stoichiometry was two molecules of MR44 per receptor monomer. Upon UV irradiation of the receptor-ligand complex, ^{125}I-MR44 was incorporated into the receptor α-subunit. From proteolytic mapping studies, we conclude that the site of ^{125}I-MR44 cross-linking is contained in the sequence αHis-186 to αLeu-199, which is part of the extracellular domain of the receptor. This sequence partially overlaps in its C-terminal region with one of the three loops that form the agonist-binding site. The agonist carbachol and the competitive antagonist α-bungarotoxin had only minor influence on the photocross-linking of ^{125}I-MR44. The site where the hydrophobic head group of ^{125}I-MR44 binds must therefore be located outside the zone that is sterically influenced by agonist bound at the nicotinic acetylcholine receptor. In binding and photocross-linking experiments, the luminal noncompetitive inhibitors ethidium and triphenylmethylphosphonium were found to compete with ^{125}I-MR44. We conclude that the polyamine moiety of ^{125}I-MR44 interacts with the high affinity noncompetitive inhibitor site deep in the channel of the nicotinic acetylcholine receptor, while the aromatic ring of this compound binds in the upper part of the ion channel (*i.e.* in the vestibule) to a hydrophobic region on the α-subunit that is located in close proximity to the agonist binding site. The region of the α-subunit labeled by ^{125}I-MR44 should therefore be accessible from the luminal side of the vestibule.

The nicotinic acetylcholine receptor (nAChR),[1] a prototypical member of the superfamily of ligand-gated ion channels, is an integral transmembrane protein with the subunit stoichiometry $\alpha_2\beta\gamma\delta$ (1–3). Each receptor subunit contains four hydrophobic sequences, which are presumed to span the plasma membrane (4, 5). The large N-terminal domain and the relatively short C-terminal part of the subunits are oriented toward the extracellular side. A large connecting loop, which is found between transmembrane sequences M3 and M4, is assumed to extend into the cytoplasm. The five subunits contribute their homologous M2 sequences to the formation of the ion channel (6), which is permeable for cations upon agonist binding. A selectivity filter formed by the five M2 helices contributes to the cation conductance properties of the channel. Three rings of negatively charged amino acid residues (7, 8) located at the constriction of the channel and on the cytoplasmic and the extracellular side of this constriction, respectively, in particular are of functional importance.

In the absence of crystals suitable for x-ray analysis, the three-dimensional structure of nAChR is investigated mainly by three approaches: electron microscopy (9, 10), site-directed mutagenesis in combination with patch clamp electrophysiology (*e.g.* Refs. 7, 11, and 12), and affinity labeling (*e.g.* Refs. 1 and 13–16). Two binding sites for agonists and competitive antagonists are located in the extracellular region, mainly on each of the two α-subunits (1) at the α-δ and α-γ interfaces (14, 17, 18). A binding site for noncompetitive inhibitors (NCIs), such as chlorpromazine, ethidium bromide, and triphenylmethylphosphonium ($TPMP^+$), has been found within the channel lumen (6, 19). These NCIs are assumed to enter the ion channel from the extracellular side and to bind deep in the channel lumen, thereby inhibiting the ion flow. Photoaffinity labels derived from well characterized NCIs have been developed to characterize the structure of the nAChR ion channel. [^{3}H]chlorpromazine and [^{3}H]$TPMP^+$ are preferentially photocross-linked to amino acid residues within the M2 transmembrane sequence of the desensitized receptor, thus demonstrating that these compounds bind deep in the ion channel and close to the selectivity filter (6, 19).

Philanthotoxin-433 (PhTX-433) is a neuroactive, polyamine-containing toxin found in the venom of the digger wasp *Philanthus triangulum* (20). Synthetic analogues of this polyamine amide, such as PhTX-343, have been shown to noncompetitively antagonize a range of ionotropic receptors (21), including nAChR (22–26). These low molecular weight compounds have a hydrophobic head group linked to a polyamine tail. At physiological pH, they are highly positively charged and, therefore, should bind to any surface with a corresponding distribution of anionic functionalities (21). The binding affinities of these compounds to nAChR are significantly influenced by modifying

* This work was supported by the European Commission, BIOMED-2 program contract BMH4-CT97-2395, Fonds der Chemischen Industrie, and the Deutsche Forschungsgemeinschaft (Sfb449). The costs of publication of this article were defrayed in part by the payment of page charges. This article must therefore be hereby marked "*advertisement*" in accordance with 18 U.S.C. Section 1734 solely to indicate this fact.

‖ To whom all correspondence should be addressed: Institut für Chemie-Biochemie, Fachbereich Biologie, Chemie, Pharmazie (AG Neurochemie), Freie Universität Berlin, Thielallee 63, 14195 Berlin, Germany. Tel.: 49-30-8385-5545; Fax: 49-30-8385-3753; E-mail: hucho@chemie.fu-berlin.de.

[1] The abbreviations used are: nAChR, nicotinic acetylcholine receptor; $TPMP^+$, triphenylmethylphosphonium; NCI, noncompetitive inhibitor; PhTX-433, philanthotoxin-433; α-BTX, α-bungarotoxin; ACh, acetylcholine; Tricine, *N*-[2-hydroxy-1,1-bis(hydroxymethyl)ethyl]glycine; HPLC, high pressure liquid chromatography; PAGE, polyacrylamide gel electrophoresis.

Downloaded from http://www.jbc.org/ by guest on July 24, 2018

their structural elements (26–28). We have synthesized a series of polyamine-containing analogues of PhTX-343 in the search for a ligand with high affinity and specificity for *Torpedo californica* nAChR for photocross-linking studies. This approach resulted in the discovery of a photoactivable compound, MR44, which binds to the nAChR with high affinity (26, 29).

In the present work, we showed that two molecules of MR44 bind with high affinity in the lumen of the nAChR ion channel. Using ^{125}I-MR44 as a photoaffinity label, we localized the site of interaction of the aromatic head group of MR44 in the vestibule of the ion channel. The sequence that was labeled by ^{125}I-MR44 was found on the α-subunit close to, but not overlapping with, the agonist-binding site. In addition, we found that bound MR44 was displaced by luminal NCIs and calcium, suggesting that the positively charged polyamine moiety of MR44 binds deep in the channel lumen at the high affinity NCI site.

EXPERIMENTAL PROCEDURES

Materials—Liquid nitrogen-frozen tissue from *T. californica* was supplied by C. Winkler (Aquatic Research Consultants, Sa Pedro). Carbamoylcholine, calcium chloride, ethidium bromide, and HEPES were from Sigma. Dithiothreitol, TPMP$^+$, and chloramine T were from Aldrich. K^{125}I was from Amersham Pharmacia Biotech. ^{125}I-Labeled α-bungarotoxin (α-BTX) was purchased from PerkinElmer Life Sciences. ArgC protease, AspN protease, LysC protease, endoglycosidase H (Endo H), and V8 protease were obtained in sequencing grade from Roche Molecular Biochemicals (Mannheim, Germany).

Synthesis and Purification of ^{125}I-Labeled MR44—MR44 was radioactively iodinated with ^{125}I using the chloramine T method (31). The mono-^{125}I derivative was isolated by reverse-phase HPLC (Waters model 626, Eschborn, Germany) on a Vydac C_{18} column applying the following linear gradient (1 ml/min): solvent A (aqueous solution containing 0.1% trifluoroacetic acid) and solvent B (acetonitrile containing 0.085% trifluoroacetic acid). The UV absorption of the eluent was determined at 305 nm, and the radioactivity of each fraction was detected using a γ-counter. ^{125}I-MR44 was characterized by matrix-assisted laser desorption-ionization mass spectrometry.

^{125}I-MR44 Binding Assays—AChR-rich membranes were prepared from frozen *T. californica* electric organ as described earlier (32). Increasing concentrations of ^{125}I-MR44 (5,000 cpm/nmol) were added to a constant amount of nAChR-rich membranes (0.3 mg/ml protein, diluted in 100 mM NaP_i, pH 7.4; total volume per sample, 200 μl) and were incubated for 45 min at room temperature. Bound ligand was separated from the free ligand by ultracentrifugation in a Beckmann tabletop ultracentrifuge for 10 min at 80,000 × *g* and 4 °C. Aliquots were withdrawn prior to centrifugation to determine the total radioactivity, and duplicate aliquots of the supernatant were removed after centrifugation to determine the free ligand concentration. Nonspecific binding was determined from bound ^{125}I-MR44 in the presence of a 100-fold molar excess of I-MR44. ^{125}I-Labeled α-BTX binding assays have been performed as described previously (33). Briefly, nAChR-rich membranes (10 μg/ml) diluted in 50 mM NaCl, 0.1% (v/v) Triton X-100, 10 mM NaP_i, pH 7.5, were incubated with increasing concentrations of ^{125}I-labeled α-BTX (0–1 μg/ml) for 45 min at room temperature (final volume 200 μl). 50 μl (duplicates) were adsorbed to DE81 filters. The filters were washed three times for 10 min with 50 mM NaCl, 0.1% (v/v) Triton X-100, 10 mM NaP_i, pH 7.5. The radioactivity of ^{125}I-labeled α-BTX bound to the filters was determined in a γ-counter. The number of α-BTX binding sites was calculated according to Hartig and Raftery (33).

For NCI and α-BTX competition experiments, ^{125}I-MR44 (9 μM; 5,000 cpm/nmol) and increasing concentrations of NCI or α-BTX were added to a constant amount of nAChR-rich membranes (0.3 mg/ml protein). In the following, the samples were treated as described above.

Calcium Competition Experiments—^{125}I-MR44 (9 μM; 5,000 cpm/nmol) was added to a constant amount of nAChR-rich membranes (0.3 mg/ml of protein) diluted in 50 mM HEPES buffer, pH 7.4 (total volume per sample, 200 μl) containing increasing concentrations of $CaCl_2$. In the following, the samples were treated as described above. Dissociation constants (K_{app} values) for competing calcium were derived from analysis of its capacity to displace ^{125}I-MR44 from its binding site at the nAChR. For calculation of K_{app} values, the binding data were plotted according to a logarithmic formula described by Herz *et al.* (34).

Cell Culture—TE671 cells were maintained in Dulbecco's modified Eagle's medium containing 4.5 g/liter glucose and supplemented with 10% (v/v) fetal calf serum, 1 mM pyruvic acid, 4 mM glutamine, 10 units/ml penicillin, and 10 μg/ml streptomycin and incubated at 37 °C in a 5% CO_2 atmosphere. Cells were divided 1:10 when they were ~75% confluent. For electrophysiology, cells were grown on glass coverslips (5 × 20 mm) in 35-mm Petri dishes and transferred to a perfusion bath mounted on the stage of an inverted microscope.

Electrophysiology—The whole-cell patch-clamp configuration was used to record whole-cell currents evoked by acetylcholine (ACh). Patch pipettes were fabricated from borosilicate glass capillaries (GC150–10; Clarke Electromedical Instruments) using a Sutter (P-97) programmable puller. Pipette resistances were ~5 megaohms when filled with 140 mM CsCl, 1 mM $CaCl_2$, 1 mM $MgCl_2$, 11 mM EGTA, and 5 mM HEPES (pH 7.2, adjusted with CsOH). The cells were constantly perfused with rat saline containing 135 mM NaCl, 5.4 mM KCl, 1 mM $CaCl_2$ 1 mM $MgCl_2$, and 5 mM HEPES (pH 7.4, adjusted with NaOH). Membrane currents were monitored using a List Electromedical L/M-EPC7 patch clamp amplifier. The patch clamp amplifier and DAD-12 Superfusion system were controlled by pClamp 5.7.2 software (Axon Instruments), which simultaneously acquired data to the hard disc of an IBM-compatible PC. Concentration-inhibition relationships for MR44 were measured to determine the IC_{50} value for inhibition of the peak current evoked by ACh (10 μM) at holding potentials (V_H) of −25, −50, and −100 mV. Experiments were performed at 18–22 °C. All data analyses were performed on an IBM-compatible PC using pClamp 5.7.2 software (Axon Instruments). Curve fitting was performed using Graphpad Prism software. IC_{50} values were determined by fitting a four-parameter logistic equation to the concentration-inhibition/response data. *p* values were determined by the unpaired Student's *t* test, and differences were considered to be significant for $p < 0.05$.

Photocross-linking Experiments—nAChR-rich membranes (50 μg) were diluted in 0.1 M NaP_i, pH 7.4, to a final receptor concentration of 140 nM. After the addition of carbachol (500 μM), the samples were incubated for 30 min at room temperature. Subsequently, TPMP$^+$, ethidium, α-BTX, or unlabeled MR44 was added, and the samples were incubated for further 30 min at room temperature. The radioactive ^{125}I-MR44 (10 μM; 250,000 cpm/nmol) was mixed with the sample solution and irradiated with UV light at 254 nm (distance, 15 cm; quartz lamp; Desaga, Heidelberg, Germany) for 15 s. Longer irradiation times resulted in a significant loss of label, presumably because the aromatic group of MR44 releases ^{125}I, and in irreversible damage of the nAChR, resulting in high molecular weight aggregates of the receptor (data not shown). Unbound ^{125}I-MR44 was separated from ^{125}I-MR44 bound to nAChR-rich membranes by centrifugation (15,000 × *g*, 15 min). The pellet was dissolved and separated by SDS-PAGE using a 10% SDS-PAG (35). The stained gel was dried, and radioactive receptor subunits were visualized by autoradiography.

Deglycosylation of nAChR Using Endo H—180 μg of nAChR-rich membranes were centrifuged after labeling with ^{125}I-MR44 and resuspended in 50 μl of 100 mM NaP_i buffer, pH 6.5. 5 μl of 1% SDS was added to this suspension, followed by 10 milliunits of Endo H in 3 μl of NaP_i buffer. As a control, buffer was added instead of Endo H. The incubation was carried out overnight at 37 °C.

Isolation of ^{125}I-Labeled α-Subunit—10 mg of nAChR (0.25 mg/ml in 0.1 M NaP_i buffer, pH 7.4) was incubated with 50 μM ^{125}I-MR44 for 30 min following UV irradiation at 254 nm for 15 s. Unbound toxin was separated from ^{125}I-MR44 bound to nAChR-rich membranes by centrifugation (15,000 × *g*, 20 min, 4 °C). The pellet was dissolved in 2 ml of gel loading buffer. For preparative gel electrophoresis (model 491 prep cell; Bio-Rad) the sample was loaded onto a 1.5-cm-wide cylindrical gel containing a 10-cm-long separating gel (10% (w/v) acrylamide) and a 3-cm-long stacking gel (3% (w/v) acrylamide). The electrophoresis was carried out overnight at 15 mA. Proteins eluting from the gel were collected in 1.5-ml fractions in 150 mM Tris/HCl, 380 mM glycine, 0.1% (w/v) SDS, pH 8.3. Fractions were assayed by SDS-PAGE and by counting the radioactivity of each fraction in a γ-counter. Fractions containing pure α-subunit were pooled. Typically, about 600 μg of α-subunit was recovered containing 600,000 cpm.

Deglycosylation of Isolated ^{125}I-Labeled α-Subunit Using Endo H—For deglycosylation of 20 μg of ^{125}I-labeled α-subunit in 70 μl of 50 mM NaP_i buffer, pH 6.5, 2 μl of 10% SDS and 10 milliunits of Endo H was added. As a control, buffer was added instead of Endo H. The incubation was carried out overnight at 37 °C.

Proteolytic Mapping Using V8 Protease—Proteolytic mapping was performed using the method of Cleveland *et al.* (36) with *S. aureus* V8 protease. The proteolytic cleavage takes place during the stacking phase of electrophoresis in the Laemmli gel system. Typically, 30 μg of pure α-subunit were lyophilized, dissolved in 25 μl of loading buffer

Downloaded from http://www.jbc.org/ by guest on July 24, 2018

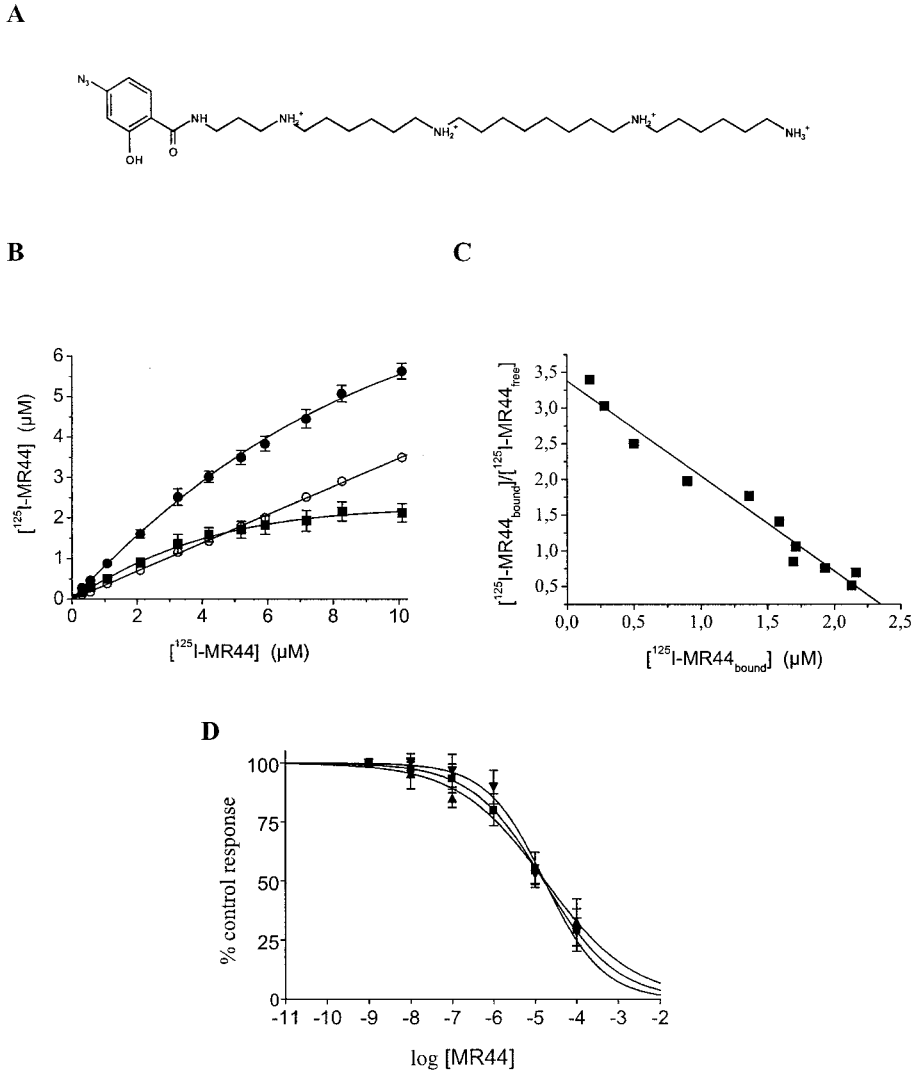

FIG. 1. *A*, chemical formula of the polymethylene tetramine MR44. *B*, binding of ^{125}I-MR44 to the nAChR. nAChR-rich membranes (0.3 mg/ml protein) were incubated with increasing concentrations of ^{125}I-MR44 (1–10 μM). The specific binding of ^{125}I-MR44 (■) was determined by subtracting the binding in the presence of a 100-fold molar excess of I-MR44 (○) from the total binding (●). Each value is the mean ± S.D. of four separate experiments *C*, Scatchard plot of ^{125}I-MR44 binding to the nAChR. The K_{app} value was 0.82 ± 0.22 μM. Using the α-BTX binding assay to determine the number of receptor monomers per μg of protein, the binding stoichiometry of MR44 was calculated to be 2.16 ± 0.18 mol of MR44/mol of nAChR monomer (n = 4). *D*, concentration-inhibition curves for MR44 inhibition of ACh (10 μM)-evoked whole TE671 cell current. V_H of −25 mV (■, n = 5), −50 mV (▲, n = 6), and −100 mV (▼, n = 7) are shown. The *solid curves* are the four-parameter logistic equation fits giving IC_{50} values of 16.1 ± 4.6 μM, 17.5 ± 7.1 μM, and 16.9 ± 4.0 μM, respectively.

(175 mM Tris/HCl, 0.1% (w/v) SDS, 5% (v/v) glycerol, pH 6.8), and incubated for 10 min at 70 °C. 4 μg of V8 protease were dissolved in 6 μl of loading buffer and added to the α-subunit. The entire sample was loaded immediately onto the stacking gel. Stacking and proteolysis were carried out for 30 min at 12 mA. Then the current was shut off for 30 min to allow further digestion by the protease, after which electrophoresis was continued. The separating gel contained 15% (w/v) acrylamide to allow adequate separation of the low molecular weight cleavage products. After Coomassie staining, the gel was dried, and radioactive peptides were visualized by autoradiography.

Proteolytic Mapping Using AspN Protease—Since the proteolytic activity of AspN protease is drastically reduced in the presence of 0.1% (w/v) SDS in the electrophoresis buffer (37), proteolytic cleavage was carried out in solution prior to electrophoretic separation of the proteolytic peptides using the Tricine gel system described by Schägger and von Jagow (38). 25 μg of ^{125}I-MR44-labeled α-subunit in 100 mM NaP_i, pH 7.5, were incubated with 2 μg of AspN protease for 27 h at 37 °C. The sample was lyophilized, dissolved in 25 μl of Tricine gel loading buffer, and incubated for 10 min at 70 °C. The samples were loaded on a Tricine gel containing a 3% spacer gel and a 16% separation gel. Electrophoresis was carried out overnight at 30 V. After Coomassie staining, the gel was dried, and radioactive peptides were visualized by autoradiography.

Proteolytic Mapping Using ArgC Protease—25 μg of ^{125}I-MR44-labeled α-subunit in 12.5 mM $CaCl_2$, 0.5% EDTA, 5 mM dithiothreitol, 100 mM Tris/HCl, pH 8.0, were incubated with 2 μg of ArgC protease for 27 h at 37 °C (39). Sample preparation, Tricine gel electrophoresis, staining of the peptides, and detection of labeled peptides were performed as described above.

Proteolytic Mapping Using LysC Protease—25 μg of ^{125}I-MR44-labeled α-subunit in 50 mM Tris/HCl, pH 8.0, 0.5% SDS were incubated with 2 μg of LysC protease for 27 h at 37 °C (40). Sample preparation, Tricine gel electrophoresis, staining of the peptides, and detection of labeled peptides were performed as described above.

Peptide Sequencing by Edman Degradation—For determination of N-terminal amino acid sequences, the peptides obtained by V8 digestion or AspN digestion and subsequent SDS-PAGE or Tricine-polyacrylamide gel electrophoresis, respectively, of ^{125}I-MR44-labeled α-subunit were blotted onto polyvinylidene difluoride membrane. After Coomassie staining, the peptides of interest were excised and submitted to Edman degradation. Protein sequence analysis was performed using a Type 473A protein sequencer (Applied Biosystems).

RESULTS

High Affinity Binding of Two Molecules of ^{125}I-MR44 per nAChR Monomer—Binding of the radioactively labeled polyamine-containing toxin MR44 (Fig. 1*A*) to the nAChR was investigated (Fig. 1, *B* and *C*). ^{125}I was introduced as radioactive label into the aromatic head group of MR44. ^{125}I-MR44 was purified by reverse-phase HPLC and analyzed by matrix-assisted laser desorption-ionization mass spectrometry (data not shown). Specific binding of ^{125}I-MR44 to nAChR-rich membranes from *T. californica* was determined by subtracting the nonspecific component from the total binding curve (Fig. 2*B*). Nonspecific binding was measured in the presence of a 100-fold molar excess of nonradioactive I-MR44. As shown in Fig. 1*B*, B_{max} was obtained at 2.11 ± 0.38 μM (n = 4). The Scatchard plot shows a straight line indicating that ^{125}I-MR44 binds to a single class of noninteracting binding sites with a K_{app} value of

Downloaded from http://www.jbc.org/ by guest on July 24, 2018

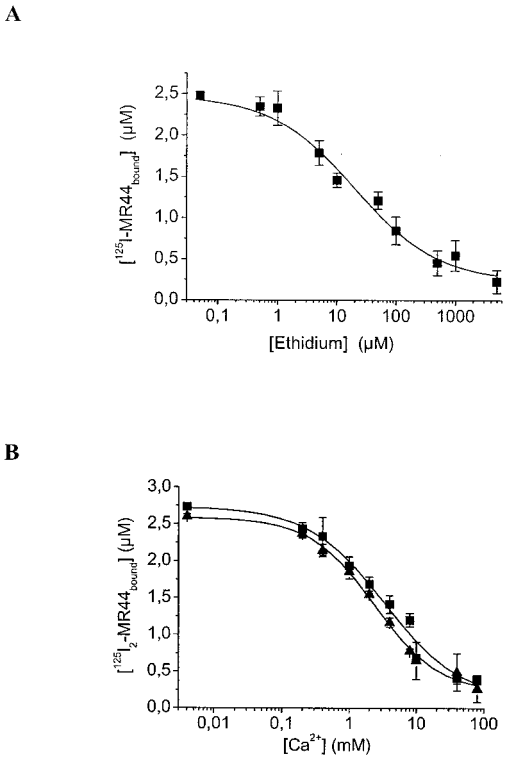

FIG. 2. *A*, ethidium displaced bound ^{125}I-MR44 at the nAChR. nAChR-rich membranes preincubated with carbachol were incubated with ^{125}I-MR44 (9 μM) in the presence of increasing concentrations of the luminal NCI ethidium. The IC_{50} value was determined to be 20.4 ± 3.6 μM (n = 3). *B*, calcium prevented binding of ^{125}I-MR44 to the nAChR. nAChR-rich membranes were incubated with ^{125}I-MR44 (9 μM) in the presence of increasing concentrations of calcium with (■) and without (▲) the agonist carbachol (n = 3). According to a logarithmic equation described by Herz *et al.* (34), the K_{app} values for calcium binding were calculated to be 12.3 ± 1.8 μM, and in the presence of carbachol they were 14.6 ± 2.2 μM.

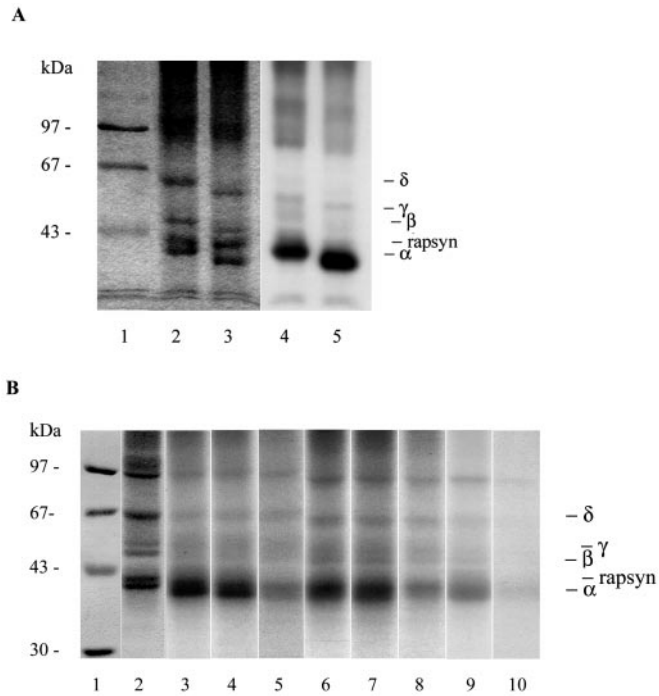

FIG. 3. *A*, effect of Endo H on nAChR photolabeled with ^{125}I-MR44. nAChR-rich membranes (30 μg each lane) were photolabeled with 10 μM ^{125}I-MR44. Samples were incubated without Endo H (*lane 2*) and with Endo H (*lane 3*) and separated on an 8% SDS-polyacrylamide gel. The gel was stained with Coomassie Blue (*lanes 1–3*), and radioactive protein bands present in *lanes 2* and *3* were visualized by autoradiography (*lanes 4* and *5*). Exposure time was typically 2 days. *B*, photoaffinity labeling of nAChR with ^{125}I-MR44. nAChR-rich membranes (50 μg each lane) were photolabeled with 10 μM ^{125}I-MR44 in the absence (*lanes 3–5*, *9*, and *10*) or the presence (*lanes 6–8*) of 500 μM carbachol and separated on an 10% SDS-polyacrylamide gel. The gel was stained with Coomassie Blue (*lane 2* shows 50 μg of nAChR-rich membranes), and radioactive protein bands were visualized by autoradiography (*lanes 3–10*). Samples were preincubated with 560 nM α-BTX (*lanes 4* and *7*) or 5 mM $TPMP^+$ (*lanes 5* and *8*) or 100 μM ethidium (*lane 9*) or 1 mM MR44 (*lane 10*). The exposure time was typically 2 days. *A* and *B*, *lane 1* shows the molecular mass markers in kDa: phosphorylase *b* (97 kDa), bovine serum albumin (67 kDa), ovalbumin (43 kDa), and carbonic anhydrase (30 kDa). Exposure time was typically 1 day.

0.82 ± 0.22 μM. In the presence of the agonist carbachol, which results in nAChR desensitization, the binding affinity of ^{125}I-MR44 was increased by a factor of 1.4, but the B_{max} value was not changed (data not shown). Using ^{125}I-labeled α-BTX in a binding assay to determine the number of receptor monomers per μg of protein (33), the binding stoichiometry of ^{125}I-MR44 was calculated to be 2.16 ± 0.18 mol of ^{125}I-MR44/mol of nAChR monomer, demonstrating that two molecules of ^{125}I-MR44 bind per receptor monomer.

Voltage-independent Inhibition of nAChR by MR44—The influence of MR44 on the agonist-mediated ion conductance of the nAChR was investigated electrophysiologically using cells that express muscle-type nAChR (cell line TE671). MR44 inhibited ACh-mediated whole-cell currents of TE671 cells with IC_{50} values of 16.1 ± 4.6 μM (n = 5), 17.5 ± 7.1 μM (n = 6), and 16.9 ± 4.0 μM (n = 7) at V_H of −25, −50, and −100 mV, respectively (Fig. 1*D*).

The NCI Ethidium Displaced Reversibly Bound ^{125}I-MR44—The well characterized luminal NCI ethidium interacts with a binding affinity of 1 μM (41) with the high affinity NCI site of the nAChR. The binding of ^{125}I-MR44 was determined in the presence of increasing concentrations of ethidium bromide. Fig. 2*A* shows that bound ^{125}I-MR44 was displaced by ethidium with an IC_{50} value of 20.4 ± 3.6 μM (n = 3). The competitive antagonist α-BTX had no influence on the binding of ^{125}I-MR44 (data not shown).

Calcium Displaced Reversibly Bound ^{125}I-MR44—It was shown previously that the NCI ethidium could be completely displaced by cations, indicating that NCIs and channel-permeating cations bind to the nAChR ion channel in a competitive manner (42). As shown in Fig. 2*B*, the divalent cation calcium displaced ^{125}I-MR44 from its binding site with an IC_{50} value of 2.4 mM. According to a logarithmic formula described by Herz *et al.* (34), the K_{app} value for calcium binding was calculated to be 12.3 ± 1.8 μM (n = 3). In the presence of carbachol, the affinity of calcium for the MR44 binding site was not significantly changed (K_{app} = 14.6 ± 2.2 μM).

^{125}I-MR44 Photolabeled the nAChR α-Subunit—For photocross-linking, ^{125}I-MR44 (10 μM) was incubated with nAChR-rich membranes. ^{125}I-MR44 was covalently cross-linked to amino acid residues facing the ligand-binding pocket by irradiation for 15 s at 254 nm. The ^{125}I-labeled receptor subunits were separated by SDS-PAGE and visualized by autoradiography (Fig. 3*A*). ^{125}I-MR44 was found to photolabel exclusively the nAChR α-subunit. No radioactivity was incorporated into the other receptor subunits at detectable levels. Since rapsyn, a 43-kDa protein associated with nAChR, migrates in the gel close to the α-subunit, the mobility of the α-subunit was increased by cleaving its carbohydrate moiety with Endo H. This endoglycosidase releases high mannose and hybrid-type *N*-linked oligosaccharides from glycoproteins (43). Deglycosylation of SDS-solubilized nAChR-rich membranes with Endo H shifted the receptor subunits, but not rapsyn, to lower molecular weights when separated by SDS-PAGE (Fig. 3*A*, *lane 3*).

Downloaded from http://www.jbc.org/ by guest on July 24, 2018

Incubation of the ^{125}I-MR44-labeled nAChR with Endo H quantitatively converted the labeled α-subunit to its high mobility form (Fig. 3*A*, *lane 5*), indicating that ^{125}I-MR44 was incorporated exclusively into the α-subunit. A 100-kDa protein (Fig. 3*A*, *lane 2*; Fig. 3*B*, *lane 2*) that most likely represents the Na^+-K^+-ATPase, was faintly labeled by ^{125}I-MR44 (Fig. 3*A*, *lane 4*; Fig. 3*B*, *lane 3*). This protein is found in nAChR-rich membrane preparations as a contamination. It has been shown previously that polyamines modulate the Na^+-K^+-ATPase and that other photolabile polyamine derivatives also photolabel this enzyme to a minor extent (26).

In the absence or presence of the agonist carbachol, photocross-linking of ^{125}I-MR44 with nAChR-rich membranes occurred with the receptor being in one of the two closed conformations, *i.e.* in the resting or in the desensitized state, respectively. In both experiments, the nAChR α-subunit was labeled (Fig. 3*B*, *lanes 3* and *6*). In the presence of well characterized luminal NCIs, such as $TPMP^+$ and ethidium bromide, ^{125}I-MR44 bound at the NCI site was completely displaced, with the labeling intensity reduced to background levels (Fig. 3*B*, *lanes 5*, *8*, and *9*). The competitive antagonist α-BTX did not significantly affect the binding of ^{125}I-MR44 (Fig. 3*B*, *lanes 4* and *7*). In the presence of α-BTX (*lane 4*) or carbachol (*lane 6*), the labeling intensity was reduced by 10–15%. Cross-linking ^{125}I-MR44 in presence of a 100-fold molar excess of the nonradioactive analogue resulted in the complete loss of labeling showing the specificity (saturability) of MR44 binding (Fig. 3*B*, *lane 10*). Without irradiation, no cross-linking was observed (data not shown).

Mapping the ^{125}I-MR44-labeled α-Subunit Using V8 Protease—The binding site of MR44 was mapped using the method described by Cleveland *et al.* (36) using *S. aureus* V8 protease, which specifically cleaves peptide bonds at the carboxyl side of glutamate residues. Limited in-gel digestion of the α-subunit with V8 protease produces preferentially four nonoverlapping fragments (44). The largest fragment, a 20-kDa peptide (V8-20), begins at αSer-173 and contains the first three membrane-spanning regions, M1, M2, and M3. The 18-kDa peptide (V8-18) is part of the extracellular domain and carries at αAsn-141 a carbohydrate residue of ~4 kDa. The 10-kDa peptide (V8-10) that begins at αAsn-339 contains the fourth membrane-spanning region, M4. The smallest fragment of 4 kDa (V8-4) represents the N-terminal part of the α-subunit.

nAChR-rich membranes were photocross-linked with ^{125}I-MR44, and the labeled α-subunit was isolated by preparative tube gel electrophoresis. The ^{125}I-MR44 labeled α-subunit was cleaved in the gel with V8 protease. Peptides generated were separated using 15% SDS-PAGE, and those fragments carrying a radioactive label were identified by autoradiography (Fig. 4*A*). Fig. 4*A*, *lanes 2–6*, show Coomassie staining of the uncleaved radiolabeled α-subunit (*lane 2*), a V8 protease digest of ^{125}I-MR44-labeled α-subunit (*lanes 3* and *4*) and of unlabeled α-subunit (*lane 5*), and V8 protease alone (*lane 6*). Using varying enzyme/substrate ratios, the limited proteolysis of the radioactively labeled and the unlabeled α-subunit reproducibly yielded identical peptide patterns. V8 cleavage of the labeled and of the unlabeled α-subunit revealed two prominent cleavage products with apparent molecular masses of about 19 kDa (V8-20) and 17 kDa (V8-18) and a smaller peptide of ~10 kDa (V8-10) (Fig. 4*A*, *lanes 3–5*). Additional minor poorly resolved cleavage products were found near the dye front of the gel. V8 protease and its proteolytic fragments appear as two major protein bands with apparent molecular masses of 29 and 27 kDa and as a 14-kDa fragment of lower intensity (Fig. 4*A*, *lane 6*). The autoradiograph of the V8-protease digest revealed that the V8-20 fragment carried the majority of the radioactive label

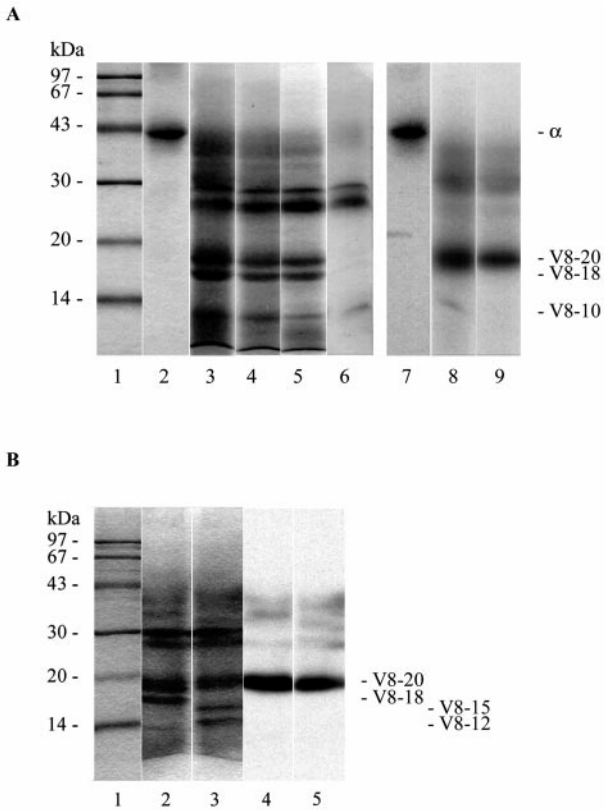

FIG. 4. *A*, proteolytic mapping of the ^{125}I-MR44-labeled nAChR α-subunit using V8 protease. After cross-linking of ^{125}I-MR44 (10 μM) with nAChR (0.2 mg/ml receptor), the ^{125}I-MR44-labeled receptor subunits were separated by preparative SDS-PAGE. The isolated ^{125}I-MR44-labeled α-subunit was incubated with V8 protease in the gel for 30 min, and peptide fragments generated were separated using 15% SDS-PAGE. *Lanes 2–5* show Coomassie staining of the radioactively labeled α-subunit (*lane 2*, 30 μg), the radioactively labeled α-subunit incubated with 6 μg of V8 protease (*lane 3*, 30 μg; *lane 4*, 15 μg), unlabeled α-subunit incubated with 4 μg of V8 protease (*lane 5*, 15 μg), and V8 protease (*lane 6*, 6 μg). *Lanes 7–9* show the localization of the radioactive peptides shown in *lanes 2–4* using autoradiography (exposure time was typically 3 days). *B*, effect of Endo H on the peptide pattern generated by V8 proteolytic cleavage of the ^{125}I-MR44-labeled nAChR α-subunit. The isolated ^{125}I-MR44-labeled α-subunit was incubated overnight without (*lane 2*) and with (*lane 3*) Endo H. The two samples were incubated with V8 protease in the gel for 30 min, and the generated peptide fragments were separated using 15% SDS-PAGE. *Lanes 2* and *3* show Coomassie staining of the peptide pattern generated by V8 digestion, and *lanes 4* and *5* show the localization of the radioactive peptides of *lanes 2* and *3*, respectively, using autoradiography (exposure time was typically 3 days). *A* and *B*, *lane 1* shows the molecular mass markers in kDa: phosphorylase *b* (97 kDa), bovine serum albumin (67 kDa), ovalbumin (43 kDa), carbonic anhydrase (30 kDa), trypsin inhibitor (20 kDa), lysozyme (14 kDa).

(Fig. 4*A*, *lanes 8* and *9*). No radioactivity was detected in the αV8-18 and αV8-10 peptides. As expected, in the absence of V8 protease the uncleaved radioactive α-subunit was found in the range of 41 kDa (Fig. 4*A*, *lane 7*).

N-terminal Amino Acid Sequencing of ^{125}I-MR44-labeled V8-20 and of Unlabeled V8-18 and V8-10—For the characterization of the peptides generated by V8 digestion, their N-terminal amino acid sequences were identified using Edman degradation. The peptides generated by in-gel V8-protease digestion were transferred to polyvinylidene difluoride membrane and visualized by Coomassie staining. Single peptide bands were excised and submitted to N-terminal amino acid sequencing. Table I shows the results of the first five sequencing cycles for each of the peptides examined. The most prominent N-terminal sequence found in the ^{125}I-MR44-labeled V8-20 peptide band started from αVal-46. As a minor signal, a

Downloaded from http://www.jbc.org/ by guest on July 24, 2018

TABLE I

N-terminal amino acid sequence analysis of ^{125}I-MR44-labeled nAChR α-subunit peptides obtained by proteolytic cleavage using V8, AspN, ArgC, or LysC proteases. Peptides were prepared and sequenced as described under "Experimental Procedures."

Protease	Peptide band	Radioactive	N-terminal amino acid sequence	Sequence indicated
V8	V8–20	Yes	x(G)E(W)V . . . (No. 1)	α173–α338
			VNQIV . . . (No. 2)	α46–α172
	V8–18	No	VNQIVE . . .	α46–α161
	V8–10	No	NxIFAD . . .	α339–α417
AspN	AspN-16	Yes	DYRGWK(H) . . .	α180–α317
	AspN-14	No	DITYxFI . . .	α200–α317
	AspN-9	No	SEHETRL . . . (No. 1)	α1–α81
			DISGKQV . . . (No. 2)	α350–α417
	AspN-7.5	No	SEHETRL . . .	α1–α70
	AspN-7	No	SEHETRL . . .	α1–α60
	AspN-4	No	DISGKQY . . . (No. 1)	α97–α137
			DGDFAIV . . . (No. 2)	α350–α388
ArgC	ArgC-10	No	IPLYFV . . . (No. 1)	α210–α301
			IM(W)TPP . . . (No. 2)	α116–α181
	Arg-4	Yes	xG(W)KHWVYYT . . . (No. 1)	α182–α209
			LPSDDV(W)LP . . . (No. 2)	α80–α115
LysC	LysC-12	No	(K)IRLPS . . .	α77–α186
	LysC-9	No	IM(W)TPP . . .	α116–α186
	LysC-8	Yes	(H)WVYYTxxPD . . . (No. 1)	α186–α242
			SDEESS . . . (No. 2)	α388–α437
	LysC-7	No	VIRPV . . .	α18–α76
	LysC-4	No	KIRLPS . . .	α77–α115

[a] x, no unambiguous assignment possible; amino acid in parentheses, only weak signal detected.

second peptide sequence was observed that most likely begins with αSer-173. The sequence was difficult to detect, since the first two amino acids of the N terminus of this peptide showed barely visible signals in the chromatograph (Tables I and II). Previous studies using limited in-gel proteolysis of the nAChR α-subunit with V8 protease (45) clearly demonstrated that V8-20 reproducibly contained two peptides beginning from αVal-46 and αSer-173, respectively, confirming the presence of the two proteolytic fragments detected in V8-20. The N-terminal sequence of unlabeled V8-18 was found to be identical with one of the V8-20 peptides (Table I). Microsequencing of unlabeled V8-10 revealed an N terminus starting from αAsn-339 (Table I). This peptide starts in the middle of the putative cytosolic loop and contains the M4 transmembrane sequence.

Effect of Endo H on ^{125}I-MR44-labeled V8-20—To identify the one of the two V8-20 peptides that carries the radioactive label, the carbohydrate moiety of the peptide starting from αVal-46 was removed to increase the mobility of this fragment when separated by SDS-PAGE. The ^{125}I-MR44-labeled α-subunit treated with and without Endo H was subsequently cleaved in the gel using V8 protease. Fig. 4*B* shows the cleavage patterns generated with respect to Coomassie staining of the gel (Fig. 4*B*, *lanes 2* and *3*) and photoincorporation of ^{125}I-MR44 as detected by autoradiography (Fig. 4*B*, *lanes 4* and *5*) after an overnight incubation without (*lanes 2* and *4*) and with (*lanes 3* and *5*) Endo H. Treatment of the α-subunit with Endo H prior to V8 cleavage altered the cleavage pattern of the peptides generated. The radioactive V8-20 band was apparently unaffected, but the intensity of the stained band seemed to be reduced (Fig. 4*B*, *lane 3*). The V8-18 peptide disappeared, and two new bands with apparent molecular masses of 15 kDa (V8-15) and 12 kDa (V8-12) were generated. These results are in good agreement with earlier findings of Pedersen *et al.* (45). These authors could show that V8-15 corresponds most likely to the deglycosylated form of an incompletely cleaved form of V8-18 that comigrated with V8-20. They also demonstrated that V8-12 was the deglycosylated from of V8-18. The autoradiograph revealed that Endo H incubation had no influence on the mobility of the ^{125}I-MR44 labeled peptide in the gel (Fig. 4*B*, *lanes 4* and *5*), demonstrating that the label and the carbohydrate moiety were associated with different V8 proteolytic fragments. These findings indicate that ^{125}I-MR44 was most likely cross-linked to the V8-20 peptide starting from αSer-173.

Mapping the ^{125}I-MR44-labeled α-Subunit Using AspN Protease—To verify the results obtained with V8 protease and to further narrow down the region of ^{125}I-MR44 cross-linking, the ^{125}I-MR44 labeled α-subunit was cleaved with AspN protease to generate a peptide pattern different from the one obtained with V8 protease. The ^{125}I-MR44-labeled α-subunit was cleaved in solution with AspN protease, and the peptides generated were separated using Tricine gel electrophoresis (Fig. 5). Coomassie-staining of the AspN proteolytic fragments revealed a pattern of peptides with molecular masses of 4–16 kDa (Fig. 5, *lane 2*). The largest of the peptides generated with a molecular mass of 16 kDa (AspN-16) was found to be exclusively photolabeled by ^{125}I-MR44 as seen in the autoradiograph (Fig. 5, *lane 3*). No radioactivity was detected in the remaining smaller peptides with apparent molecular masses of 14 kDa (AspN-14), 9 kDa (AspN-9), 7.5 kDa (AspN-7.5), 7 kDa (AspN-7), and 4 kDa (AspN-4).

N-terminal Amino Acid Sequencing of ^{125}I-MR44-labeled AspN-16 and of Unlabeled AspN-14, AspN-9, AspN-7.5, AspN-7 and AspN-4—To localize these peptides in the known primary structure of the α-subunit, the radioactively labeled fragment AspN-16 and the other unlabeled fragments AspN-14 to AspN-4 were isolated and submitted to Edman degradation as described above. Table II shows the results of the sequencing cycles. The N-terminal sequence of AspN-16, which carried the cross-linked ^{125}I-MR44, was found to begin with αAspN-180 (Tables I and II). This finding confirms our result obtained with V8 protease, which demonstrated that the radioactive label is localized within the 19-kDa peptide of the α-subunit beginning with αSer-173. Most remarkably, the N-terminal sequence of the unlabeled peptide migrating at 14 kDa was determined to begin with αAsp-200 (Table I). Consequently, ^{125}I-MR44 must be photoincorporated into the 2.5-kDa peptide αAsp-180 to αLeu-199. Microsequencing of the unlabeled AspN-9 revealed two peptide sequences beginning with αSer-1 and αAsp-350, respectively. Therefore, one of the peptides represents the N terminus presumably ending at αSer-82, and the other corre-

Downloaded from http://www.jbc.org/ by guest on July 24, 2018

TABLE II

N-terminal amino acid sequence analysis of ^{125}I-MR44-labeled peptides obtained by cleavage of the labeled α-subunit using V8, AspN, ArgC, or LysC proteases. The αV8–20, αAspN-16, αArgC-4, and αLysC-8 proteolytic peptide carried a radioactive label. Peptides were prepared and sequenced as described under "Experimental Procedures."

Cycle	V8–20 (No. 1)		V8–20 (No. 2)		AspN-16		ArgC-4 (No. 1)		ArgC-4 (No. 2)		LysC-8 (No. 1)		LysC-8 (No. 2)	
	Residue	Amount	Residue	Amount	Residue	Amount	Residue	Amount	Residue	Amount	Residue	Amount	Residue	Amount
		pmol		*pmol*		*pmol*		*pmol*		*pmol*		*pmol*		*pmol*
1	αVal-46	16.56	αSer-173	x[a]	αAsp-180	3.25	αArg-182	x	αLeu-80	15.58	αHis-186	0.60	αSer-388	5.68
2	αAsn-47	20.46	αGly-174	4.10	αTyr-181	1.55	αGly-183	11.88	αPro-81	13.06	αTrp-187	1.95	αAsp-389	6.93
3	αGln-48	19.94	αGlu-175	13.24	αArg-182	2.08	αTrp-184	2.09	αSer-82	8.38	αVal-188	3.31	αGlu-390	4.13
4	αIle-49	9.36	αTrp-176	2.57	αGly-183	2.13	αLys-185	3.07	αAsp-83	11.76	αTyr-189	2.73	αGlu-391	7.63
5	αVal-50[b]	12.06	αVal-177[b]	12.06	αTrp-184	2.03	αHis-186	1.47	αAsp-84	10.42	αTyr-190	4.29	αSer-392	10.13
6					αLys-185	0.58	αTrp-187	1.98	αVal-85	10.04	αThr-191	2.96	αSer-393	10.27
7					αHis-186	0.44	αVal-188	12.36	αTyp-86	2.00	αCys-192	x	αGln-394	2.27
8					αTrp-187	1.84	αTyr-189	4.43	αLeu-87	7.95	αCys-193	x	αAla-395	3.62
9					αVal-188	0.93	αTyr-190	5.22	αPro-88	4.65	αPro-194	2.37	αAla-396	4.19

[a] x, peak was not integrated.
[b] Indication to one of these two sequences not possible.

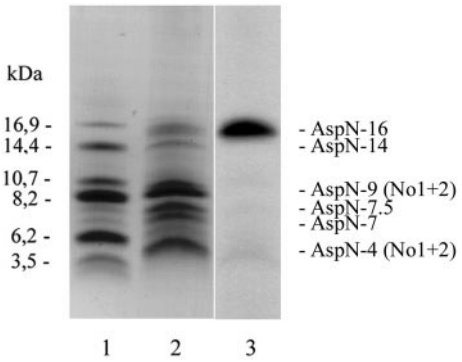

FIG. 5. **Proteolytic mapping of the ^{125}I-MR44 labeled nAChR α-subunit using AspN protease.** After cross-linking of ^{125}I-MR44 (10 μM) with nAChR (0.2 mg/ml receptor), the ^{125}I-MR44-labeled receptor subunits were separated by preparative SDS-PAGE. The isolated ^{125}I-MR44 labeled α-subunit was incubated overnight with AspN protease, and the generated peptide fragments were separated using Tricine-polyacrylamide gel electrophoresis with 3% spacer and 16% separation gel. *Lane 2* shows the Coomassie-stained peptides that were generated by incubation of the ^{125}I-MR44-labeled α-subunit (25 μg) with AspN protease (2 μg). *Lane 3* shows the corresponding autoradiograph to localize radioactive peptides (exposure time was typically 2 days). *Lane 1* shows the molecular mass markers in kDa on the ordinate: globine (16.9 kDa), globine I + II (14.4 kDa), globine I + III (10.7 kDa), globine I (8.2 kDa), globine II (6.2 kDa), glucagon (3.5 kDa).

sponds to the C terminus with part of the putative cytosolic loop including the M4 transmembrane sequence (Table I). AspN-7.5 (AspN-7) and AspN-4 (number 2) were identified as smaller cleavage products of AspN-9 (number 1) and AspN-4 (number 2), respectively. AspN-4 contained a second sequence starting from αAsp-97, which is part of the extracellular domain. All unlabeled AspN proteolytic fragments were nonoverlapping with the 20-amino acid sequence αAsp-180 to αLeu-199.

Mapping the ^{125}I-MR44-labeled α-Subunit Using ArgC Protease—Using ArgC protease, an enzyme that cleaves peptide bonds at the C-terminal side of arginine residues, a cleavage of the region suggested to be labeled by the experiments described above on the α-subunit into fragments of 12 kDa (α80–182), 3.4 kDa (α183–209), and 10 kDa (α210–301), respectively, is predicted. When the ^{125}I-MR44-labeled α-subunit was subjected to cleavage using this protease and the peptides were separated by Tricine gel electrophoresis, peptides in the molecular mass range of 4–15 kDa were found in the Coomassie-stained gel (Fig. 6*A*). In the autoradiograph, a single radioactively labeled peptide band of about 4 kDa (ArgC-4) was detected. The other peptides generated carried no radioactivity (Fig. 6*A*, *lane 3*).

N-terminal Amino Acid Sequencing of ^{125}I-MR44-labeled ArgC-4 and of Unlabeled ArgC-15, ArgC-10, and ArgC-9—N-terminal amino acid sequencing of the ^{125}I-MR44 labeled ArgC-4 fragment yielded two sequences starting at their N-terminal ends with αArg-182 and αLeu-80, respectively (Tables I and II). One of the fragments, α80–115, had previously been shown to be nonradioactive using V8 and AspN proteases. Most importantly, the second sequence, which therefore must carry the radioactive label, starts from αArg-182, confirming the site of ^{125}I-MR44 photoincorporation that was already suggested from our V8 and AspN digest experiments. The N-terminal sequences of unlabeled ArgC-10 and ArgC-9 were found to begin from αIle-210 and αIle-116, respectively (Table I). The unlabeled 15-kDa peptide was identified as a proteolytic fragment of the ArgC protease. The specificity of ArgC is primarily to arginine residues, although hydrolysis proceeds to a minor degree also after lysine residues (39) and occasionally after aromatic residues (47). As a result, the labeled α-subunit was cleaved at the C-terminal side of αLys-116 and αTyr-181 (N-terminal side of αArg-182). Taken together with the results obtained with V8 and AspN protease, this observation allows us to locate the site of ^{125}I-MR44 cross-linking to the sequence αArg-182 to αLeu-199.

Mapping the ^{125}I-MR44-labeled α-Subunit Using LysC Protease—The sequence labeled by ^{125}I-MR44 contains at position 185 a lysine residue. LysC protease, an protease that cleaves the peptide bond after lysine residues (40), was therefore used to cleave the labeled α-subunit. The peptides generated were subsequently separated using Tricine gel electrophoresis. The Coomassie-stained gel showed peptides in the molecular mass range of 7–14 kDa (Fig. 6*B*). The autoradiograph identified a single radioactive peptide of about 8 kDa (LysC-8), while the other peptide generated carried no radioactivity (Fig. 6*B*, *lane 3*).

N-terminal Amino Acid Sequencing of ^{125}I-MR44-labeled LysC-8 and of Unlabeled LysC-12, LysC-10, LysC-7, and LysC-6—Sequencing of the N terminus of the radioactively labeled LysC-8 fragment yielded a single sequence starting from His-186 (Tables I and II). The other unlabeled fragments LysC-12, LysC-10, and LysC-7 were found to start from αSer-77, αIle-116, and αVal-18, respectively. LysC-4 was identified as a smaller cleavage product of LysC-12 (Table I). All identified nonradioactive peptides generated by proteolytic cleavage with V8, AspN, ArgC, or LysC proteases represent sequences of the α-subunits that were nonoverlapping with the sequence αHis-186 to αLeu-199. These findings allow us to further narrow down the site of modification to the amino acid stretch αHis-186 to αLeu-199.

Attempts to identify the precise site of modification within this amino acid stretch by using the release of radioactivity during Edman sequencing failed, since the radioactive photoaf-

Downloaded from http://www.jbc.org/ by guest on July 24, 2018

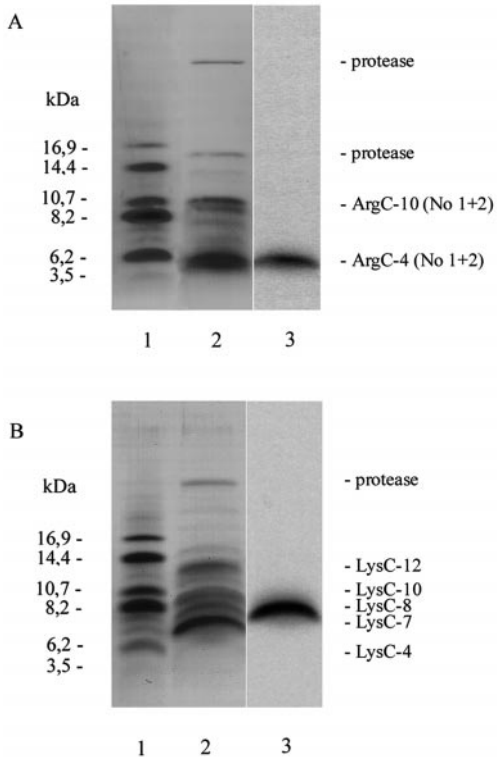

FIG. 6. **Proteolytic mapping of the ^{125}I-MR44-labeled nAChR α-subunit using ArgC protease (*A*) and LysC protease (*B*).** After cross-linking of ^{125}I-MR44 (10 μM) with nAChR (0.2 mg/ml receptor), the ^{125}I-MR44-labeled receptor subunits were separated by preparative SDS-PAGE. The isolated ^{125}I-MR44-labeled α-subunit was incubated overnight with ArgC protease (*A*) or LysC protease (*B*), and the generated peptide fragments were separated using Tricine-polyacrylamide gel electrophoresis with 3% spacer and 16% separation gel. *Lane 2* (*A* and *B*) shows the Coomassie-stained peptides that were generated by incubation of the ^{125}I-MR44-labeled α-subunit (25 μg) with ArgC protease (*A*; 2 μg) or LysC protease (*B*; 2 μg). *Lane 3* (*A* and *B*) shows the corresponding autoradiograph to localize radioactive peptides (exposure time was typically 2 days). Lane 1 (*A* and *B*) shows the molecular mass markers in kDa on the ordinate: globine (16.9 kDa), globine I + II (14.4 kDa), globine I + III (10.7 kDa), globine I (8.2 kDa), globine II (6.2 kDa), glucagon (3.5 kDa).

finity label is not stable under the chemical conditions of the Edman degradation cycle. ^{125}I-MR44 quantitatively releases ^{125}I from the aromatic ring in the first sequencing step during alkaline and acidic treatment (data not shown).

DISCUSSION

The architecture of ligand-gated ion channels can be explored using photoaffinity derivatives of high affinity ligands. The aim of the present studies was to identify amino acid residues facing the ligand-binding site of *T. californica* nAChR and thereby to obtain information on the structure of the luminal surface of the channel gated by this receptor. We have used a newly developed polyamine-containing toxin carrying a hydrophobic head group in photocross-linking experiments. The novel photoaffinity label MR44 was first characterized electrophysiologically and by binding studies and was subsequently used to map the ligand binding site in the lumen of the nAChR ion channel.

Using fluorescent titration, we have shown recently that PhTX analogues including MR44 interact with the fluorescent NCI ethidium bound to the high affinity NCI site in the desensitized state of the nAChR (26). Like most amine NCIs containing aromatic or aliphatic rings, such as chlorpromazine, meproadifen, and TPMP$^+$ (41, 48, 49), MR44 was found to bind with higher affinity in the presence of the agonist carbachol, *i.e.* when the nAChR is in its desensitized closed state, as compared with the resting closed conformation. Since MR44 causes a voltage-independent block of AChR-induced ion flow, MR44 presumably acts as inhibitor of the closed channel conformation rather than as an open channel blocker. Unlike other classical NCIs, which show a binding stoichiometry of 1:1, we found that two molecules of MR44 were bound per receptor monomer. In a recent study, the same binding stoichiometry was observed for another PhTX derivative, N_3-phenyl-$^{125}I_2$-PhTX-343-lysine (26). MR44 has two functional moieties; a long positively charged polyamine tail on the one side and an aromatic head group on the other. It is most likely that these two structural elements of the molecule, although both contribute to the binding affinity, bind at different sites within the receptor lumen.

For photocross-linking, ^{125}I-MR44 was incubated with nAChR-rich membranes and subsequently irradiated with UV light to generate a reactive nitrene species that efficiently cross-links to any amino acid residues nearby that are facing the binding site. The finding that ^{125}I-MR44 photolabeled the receptor α-subunit suggests that the aromatic head groups of the two MR44 bound in the channel lumen most likely interact each with one of the α-subunits, since this part of MR44 carries the photolabile group.

To localize the polyamine-binding site at the nAChR in its resting closed state, the regions of the α-subunit that incorporated ^{125}I-MR44 were mapped by proteolytic cleavage using V8 (36, 45), AspN (37), ArgC (39), and LysC proteases (40). The N termini of peptides generated were microsequenced and localized in the known primary structure of the *Torpedo* nAChR α-subunit (4). When using limited V8 proteolysis, the majority of the radioactivity was detected in a 19-kDa proteolytic fragment. Microsequencing and Endo H treatment identified two fragments in the V8-20 peptide band beginning with αVal-46 and αSer-173, respectively. These data correspond to earlier findings of Pedersen *et al.* (45) demonstrating that the V8-20 band contained two comigrating fragments: a carbohydrate-containing peptide starting from αVal-46 and an unglycosylated peptide beginning from αSer-173. Removal of the oligosaccharide moiety by Endo H had no influence on the mobility of the radioactively labeled V8-20 peptide, indicating that ^{125}I-MR44 photolabels the fragment beginning with αSer-173. To confirm this finding, AspN protease was used to cleave the ^{125}I-MR44 labeled α-subunit at sites different from that cleaved by V8 protease. An AspN proteolytic fragment of 16 kDa was found to carry the radioactive label. Microsequencing of this peptide revealed a single sequence beginning from αAsp-180, confirming the results obtained with V8 protease. The N-terminal sequence of the unlabeled proteolytic fragment migrating at 14 kDa was identified to start from αAsp-200. Thus, the cross-linked ^{125}I-MR44 must be located within a stretch of 20 amino acid residues from αAsp-180 to αLeu-199. Cleavage of the ^{125}I-MR44-labeled α-subunit with ArgC protease generated a peptide pattern with only one peptide labeled of about 4 kDa. N-terminal amino acid sequencing identified two proteolytic fragments starting with Arg-182 and Leu-80, respectively. The peptide beginning with αLeu-80 was shown to be nonradioactive using V8, AspN, and LysC proteases. Consequently, ^{125}I-MR44 must be cross-linked to the ArgC-4 fragment starting with Arg-182, confirming the region of ^{125}I-MR44 photoincorporation suggested from the V8 and AspN digest experiments. The sequence αArg-182 to αLeu-199 labeled by ^{125}I-MR44 contains a lysine residue in position 185. Therefore, LysC protease was used to cleave the labeled α-subunit. In mapping experiments using LysC protease, we further narrowed down the site of modification to the amino acid stretch αHis-186 to αLeu-199.

Downloaded from http://www.jbc.org/ by guest on July 24, 2018

This sequence is located in the large N-terminal domain of the α-subunit; it is found close to one of the three loops that contribute to the agonist-binding site. Photoaffinity reagents and site-directed mutagenesis have been utilized in previous studies to identify amino acid residues facing the agonist-binding domain. Three discrete regions on the α-subunit primary structure have been identified: αTrp-86 to αTyr-93 (loop A), αTrp-147 to αTyr-150 (loop B), and αTyr-190 to αTyr-198 (loop C; Refs. 50–54). Two additional regions on each of the neighboring δ- and γ-subunits were found to contribute to the binding site (loop D and E; Refs. 55–57). Based on these data, a spatial model has been developed according to which three sequences of the α-subunit and two sequences of the neighboring δ- and γ-subunits form the agonist binding pockets of nAChR (58, 59). The amino acid residues forming loop C overlap in the C-terminal region at least partially with the sequence αHis-186 to αLeu-199 labeled by ^{125}I-MR44. Since the agonist carbachol or the competitive antagonist α-BTX had only minor influence on the photocross-linking yield of ^{125}I-MR44, the site of interaction between the aromatic ring of ^{125}I-MR44 and the nAChR should be found outside the zone that is sterically influenced by any bound agonist contacting αTyr-190, αCys-192, αCys-193, and αTyr-198. Therefore, the site of interaction of the aromatic head group of ^{125}I-MR44 lies presumably within the hydrophobic sequence HWVY (residues α186–189) containing three aromatic amino acid residues. Receptor desensitization induced by carbachol might influence the accessibility of those residues that react in the resting channel state with ^{125}I-MR44 without affecting the binding affinity of the whole molecule.

From various structure-activity relationship studies, it is obvious that the aromatic moiety of PhTX derivatives has a significant influence on the binding affinity of these compounds (26, 27). Their binding properties were considerably improved by increasing the size and hydrophobicity of the head group. The finding that ^{125}I-MR44 photolabeled a sequence of the α-subunit in which aromatic amino acid residues are accumulated is in line with the observation that PhTX derivatives that carry a large, hydrophobic head group bind with increased affinity to the nAChR (26, 27).

Since the photolabile azido residue of MR44 is located at its aromatic head group, the site of ^{125}I-MR44 cross-linking identifies the region to which this hydrophobic part of the molecule binds. In contrast, the site of interaction of the conformationally flexible carbon chain can be less exactly determined. Due to its positively charged -NH_2 groups interspersed with hydrophobic -CH_2 groups, the polyamine chain is expected to preferentially interact with acidic and hydrophobic amino acid side chains, respectively. This is similar to the active site of bacterial polyamine binding proteins (60). In previous studies, it was suggested that the positively charged polyamine tail binds in the lumen of the nAChR ion channel to the negatively charged amino acids that are part of the selectivity filter (27). To examine the site to which the polyamine moiety of MR44 binds, the well characterized luminal NCI ethidium was used in various displacement assays. Previous studies located the ethidium-binding site at the high affinity NCI site deep in the ion channel of the nAChR, presumably close to the M2 helix (34, 50). Our finding that the quaternary amine ethidium competed with ^{125}I-MR44 supports the view that the positively charged polyamine tail of MR44 is oriented toward the narrow part of the ion channel lumen. Using the NCI ethidium as a fluorescent probe at the nAChR, we determined recently the binding affinities of various PhTX derivatives including MR44. Increasing concentrations of MR44 reduced the fluorescence of bound ethidium, indicating that MR44 displaced ethidium from its binding site. This observation corresponds well to the results presented here that ethidium competes with bound ^{125}I-MR44 and that photoincorporation of ^{125}I-MR44 was prevented in the presence of ethidium and $TPMP^+$. Ethidium was still displaced by MR44 even when allosteric transitions within the nAChR had been abolished by covalent cross-linking (26). This finding strongly suggests that MR44 interacts with ethidium in a direct competitive manner at an overlapping luminal binding site. Channel-permeating cations, such as calcium, are known to bind to sites within the nAChR ion channel that sterically overlap with the high affinity NCI site (42). Using calcium in direct binding experiments, we could show that ^{125}I-MR44 bound to the nAChR was completely displaced by calcium. This observation indicates a strong influence of polar electrostatic interactions between ^{125}I-MR44 and the NCI site of the nAChR. A site of negative charges located deep in the lumen of the nAChR ion channel that might interact with the positively charged polyamine tail of ^{125}I-MR44 could provide the acidic amino acid residues of the selectivity filter as suggested in earlier studies (27). To summarize, the polyamine moiety of MR44 interacts with the high affinity NCI site of the nAChR, while the aromatic ring of this compound binds to the upper part of the ion channel, *i.e.* in the vestibule, and therefore to a hydrophobic region on the α-subunit that is located in close proximity to the loop C of the agonist binding site and is accessible from the water-filled lumen of the channel.

Acknowledgment—We thank Hermann Bayer for help with nAChR preparations and for excellent technical assistance.

REFERENCES

1. Changeux, J.-P. (1990) *Fidia Res. Found. Neurosci. Award Lect.* **4,** 21–168
2. Karlin, A., and Akabas, M. H. (1995) *Neuron* **15,** 1231–1244
3. Hucho, F., Tsetlin, V., and Machold, J. (1996) *Eur. J. Biochem.* **239,** 539–557
4. Noda, M., Takahashi, H., Tanabe, T., Toyosato, M., Furutani, Y., Hirose, T., Asai, M., Inayama, S., Miyata, T., and Numa, S. (1982) *Nature* **299,** 793–797
5. Noda, M., Takahashi, H., Tanabe, T., Toyosato, M., Kikyotani, S., Furutani, Y., Hirose, T., Takashima, H., Inayama, S., Miyata, T., and Numa, S. (1983) *Nature* **302,** 532–538
6. Hucho, F., Oberthür, W., and Lottspeich, F. (1986) *FEBS Lett.* **205,** 137–142
7. Imoto, K., Busch, C., Sakmann, B., Mishina, M., Konno, T., Nakai, J., Bujo, H., Mori, Y., Fukudo, K., and Numa, S. (1988) *Nature* **335,** 645–648
8. Konno, T., Busch, C., Von Kitzing, E., Imoto, K., Wang, F., Nakai, J., Mishina, M., Numa, S., and Sakmann, B. (1991) *Proc. R. Soc. Lond. B. Biol. Sci.* **244,** 69–79
9. Unwin, N. (1995) *Nature* **373,** 37–43
10. Miyazawa, A., Fujiyoshi, Y., Stowell, M., and Unwin, N. (1999) *J. Mol. Biol.* **288,** 765–786
11. Villarroel, A., Herlitze, S., Witzemann, V., Koenen, M., and Sakmann, B. (1992) *Proc. R. Soc. Lond. B. Biol. Sci.* **249,** 317–324
12. Corringer, P.-J., Bertrand, S., Galzi, J.-L., Devillers-Thiéry, A., Changeux, J.-P., and Bertrand, D. (1999) *Neuron* **22,** 831–843
13. Sine, S. M, Kreienkamp, H. J., Bren, N., Maeda, R., and Taylor, P. (1995) *Neuron* **15,** 205–211
14. Machold, J., Utkin, Y., Kirsch, D., Kaufmann, R., Tsetlin, V., and Hucho, F. (1995) *Proc. Natl. Acad. Sci. U. S. A.* **92,** 7282–7286
15. Chiara, D. C., and Cohen, J. B. (1997) *J. Biol. Chem.* **272,** 32940–32950
16. Wilson, G. G., and Karlin, A. (1998) *Neuron* **20,** 1269–1281
17. Blount, P., and Merlie, J. P. (1989) *Neuron* **3,** 349–357
18. Pedersen, S. E., and Cohen, J. B. (1990) *Proc. Acad. Natl. Sci. U. S. A.* **87,** 2785–2789
19. Giraudat, J., Dennis, M., Heidmann, T., Chang, J. Y., and Changeux, J.-P. (1986) *Proc. Natl. Acad. Sci. U. S. A.* **83,** 2719–2723
20. Eldefrawi, A. T., Eldefrawi, M. E., Konno, K., Mansour, N. A., Nakanishi, K., Oltz, E., and Usherwood, P. N. R. (1988) *Proc. Natl. Acad. Sci. U. S. A.* **85,** 4910–4913
21. Usherwood, P. N. R., and Blagbrough, I. R. (1991) *Pharmacol. Ther.* **52,** 245–268
22. Ragsdale, D., Gant, D. B., Anis, N. A., Eldefrawi, A. T., Eldefrawi, M. E., Konno, K., and Miledi, R. (1989) *J. Pharmacol. Exp. Ther.* **251,** 156–156
23. Rozental, R., Scoble, G. T., Albuquerque, E. X., Idriss, M., Sherby, S., Sattelle, D. R., Nakanishi, K., Konno, K., Eldefrawi, A. T., and Eldefrawi, M. E. (1989) *J. Pharmocol. Exp. Ther.* **349,** 123–130
24. Shao, Z., Mellor, I. S., Brieley, M. J., Harris, J., and Usherwood, P. N. R. (1998) *J. Pharmacol. Exp. Ther.* **286,** 1269–1276
25. Jayaraman, V., Usherwood, P. N. R., and Hess, G. P. (1998) *Biochemistry* **38,** 11406–11414
26. Bixel, M. G., Krauss, M., Liu, Y., Bolognesi, M. L., Rosini, M., Mellor, I. S., Usherwood, P. N. R., Melchiorre, C., Nakanishi, K., and Hucho, F. (2000) *Eur. J. Biochem.* **267,** 110–120
27. Anis, N., Sherby, S., Goodnow, R., Niwa, M., Konno, K., Kallimopoulos, T.,

Downloaded from http://www.jbc.org/ by guest on July 24, 2018

Bukownik, R., Nakanishi, K., Usherwood, P., Eldefrawi, A., and Eldefrawi, M. (1995) *J. Pharmacol. Exp. Ther.* **254,** 764–773
28. Nakanishi, K., Huang, X., Jiang, H., Liu, Y., Fang, K., Huang, D., Choi, S.-K., Katz, E., and Eldefrawi, M. (1997) *Bioorg. Med. Chem.* **5,** 1969–1988
29. Rosini, M., Budriesi, R., Bixel, M. G., Bolognesi, M. L., Chiarini, A., Hucho, F., Krogsgaard-Larsen, P., Mellor, I., Minarini, A., Tumiatti, V., Usherwood, P. N. R., and Melchiorre, C. (1999) *J. Med. Chem.* **42,** 5212–5223
30. Galzi, J.-L., Bertrand, S., Corringer, P.-J., Changeux, J.-P., and Bertrand, D. (1996) *EMBO J.* **15,** 5824–5832
31. Greenwood, F. C., Hinter, W. M., and Glover, J. S. (1963) *Biochem. J.* **89,** 114–121
32. Schiebler, W., Lauffer, L., and Hucho, F. (1977) *FEBS Lett.* **81,** 39–41
33. Hartig, P. R., and Raftery, M. A. (1979) *Biochemistry* **18,** 1146–1150
34. Herz, J. M., Johnson, D. A., and Taylor, P. (1987) *J. Biol. Chem.* **262,** 7238–7247
35. Laemmli, U. K. (1970) *Nature* **227,** 680–685
36. Cleveland, D. W., Fischer, S. G., Kirschner, M. W., and Laemmli, U. K. (1977) *J. Biol. Chem.* **252,** 1102–1106
37. Drapeau, G. R. (1980) *J. Biol. Chem.* **255,** 839–840
38. Schägger, H., and von Jagow, G. (1987) *Anal. Biochem.* **166,** 368–379
39. Mitchell, W. M., and Harrington, W. F. (1968) *J. Biol. Chem.* **243,** 4683–4692
40. Jekel, P. A., Weijer, W. J., and Beintema, J. J. (1983) *Anal. Biochem.* **134,** 347–354
41. Sterz, R., Hermes, M., Peper, K., and Bradley, R. J. (1982) *Eur. J. Pharmacol.* **80,** 393–399
42. Herz, J. M., Kolb, S. J., Erlinger, T., and Schmid, E. (1991) *J. Biol. Chem.* **266,** 16691–16698
43. Varki, A., and Kornfeld, S. (1983) *J. Biol. Chem.* **258,** 2808–2818
44. White, B. H., and Cohen, J. B. (1988) *Biochemistry* **27,** 8741–8751
45. Pedersen, S. E., Dreyer, E. B., and Cohen, J. B. (1986) *J. Biol. Chem.* **261,** 13735–13743
46. Tetaz, T., Morrison, J. R., Andreou, J., and Fidge, N. H. (1990) *Biochem. Int.* **22,** 561–566
47. Ullmann, D., and Jakubke, H. D. (1994) *Eur. J. Biochem.* **223,** 865–872
48. Lauffer, L., and Hucho, F. (1982) *Proc. Natl. Acad. Sci. U. S. A.* **79,** 2406–2409
49. Krauss, M., Korr, D., Hermann, A., and Hucho, F. (2000) *J. Biol. Chem.* **275,** 30196–30201
50. Pratt, M. B., Pedersen, S. E., and Cohen, J. B. (2000) *Biochemistry* **39,** 11452–11462
51. Kao, P. N., and Karlin, A. (1986) *J. Biol. Chem.* **261,** 8085–8088
52. Dennis, M., Giraudat, J., Kotzyba-Hibert, F., Goeldner, M., Hirth, C., Chang, J. Y., Lazure, C., Chretien, B., and Changeux, J.-P. (1988) *Biochemistry* **27,** 2346–2357
53. Galzi, J. L., Revah, F., Black, D., Goeldner, M., Hirth, C., and Changeux, J.-P. (1990) *J. Chem. Biol.* **265,** 10430–10437
54. Cohen, J. B., Sharp, S. D., and Liu, W. S. (1991) *J. Biol. Chem.* **266,** 23354–23364
55. Czaijkowski, C., and Karlin, A. (1995) *J. Biol. Chem.* **270,** 3160–3164
56. Prince, R. J., and Sine, S. M. (1996) *J. Biol. Chem.* **271,** 25770–25777
57. Martin, M. D., and Karlin, A. (1997) *Biochemistry* **36,** 10742–10750
58. Bertrand, D., and Changeux, J.-P. (1995) *Neurosciences* **7,** 75–90
59. Changeux, J.-P., Bertrand, D., Corringer, P.-J., Dehaeme, S., Edelstein, S., Léna, C., Le Novère, N., Narubio, L., Picciotto, M., and Zoli, M. (1998) *Brain Res. Rev.* **26,** 198–216
60. Sugiyama, S., Matsuo, Y., Maenaka, K., Vassylyev, D. G., Matsushima, M., Kashiwagi, K., Igarashi, K., and Morikawa, K. (1996) *Protein Sci.* **5,** 1984–1990

Downloaded from http://www.jbc.org/ by guest on July 24, 2018

Location of the Polyamine Binding Site in the Vestibule of the Nicotinic Acetylcholine Receptor Ion Channel

M. Gabriele Bixel, Christoph Weise, Maria L. Bolognesi, Michela Rosini, Matthew J. Brierly, Ian R. Mellor, Peter N. R. Usherwood, Carlo Melchiorre and Ferdinand Hucho

J. Biol. Chem. 2001, 276:6151-6160.
doi: 10.1074/jbc.M008467200 originally published online December 4, 2000

Access the most updated version of this article at doi: 10.1074/jbc.M008467200

Alerts:
- When this article is cited
- When a correction for this article is posted

Click here to choose from all of JBC's e-mail alerts

This article cites 60 references, 24 of which can be accessed free at
http://www.jbc.org/content/276/9/6151.full.html#ref-list-1

Downloaded from http://www.jbc.org/ by guest on July 24, 2018